

# Lateral resolution limits in microscopy with entangled photon pairs

Maria Gieysztor,<sup>1</sup> Joshua Nepinak,<sup>2</sup> Christopher J. Pugh,<sup>1,2,3</sup> and Piotr Kolenderski<sup>1,\*</sup>

<sup>1</sup>*Faculty of Physics, Astronomy and Informatics, Nicolaus Copernicus University, Grudziadzka 5, 87-100 Toruń, Poland*

<sup>2</sup>*Department of Physics and Astronomy, Brandon University, 270-18 Street, Brandon, MB, R7A 6A9, Canada*

<sup>3</sup>*Newman Theological College, 10012-84 Street NW, Edmonton, AB, T6A 0B2, Canada*

In this work a theoretical analysis of the lateral resolution limits of an optical setup in a microscopy setting with an entangled photons pair source is performed. A correlated biphoton wavefunction of a general Gaussian form, is propagated through a given experimental setup. Next, the signal photon's spatial mode profile width and central position are investigated in the heralding scenario, which means the information about the idler photon is not neglected. The impact of the correlations on the signal photon's spatial mode profile is compared in the heralding and non-heralding scenario. A realistic experimental scheme is considered, taking into account finite size optics and single photon detectors. This method allows us to significantly alleviate the photon loss problem in the optical setup which is a crucial factor limiting practical applications of single photon based techniques. It is achieved by an effect similar to phase shaping introduced by spatial light modulators.

PACS numbers: 42.50.Ex, 42.65.Lm, 42.50.Dv, 42.79.Sz

Keywords: parametric down-conversion; spatial correlation; photon-pair sources; transverse resolution

## I. INTRODUCTION

The lateral resolution of different optical microscopy and imaging setups is bound by finite size optics and expressed by the fundamental diffraction limit  $0.61\lambda/NA$  in the Rayleigh criterion [1, 2], where  $\lambda$  is the wavelength of the illuminating beam and NA stands for the numerical aperture of the optical setup.

For visible wavelengths and typical optics this limit is of the order of 200 nm. There are a variety of methods designed to improve the resolution, however, their applicability is limited to certain experimental configurations. In confocal microscopy, for example, an additional imaging system combined with a pinhole [3] helps to reduce the size of the illumination volume. Further enhancement can be achieved when harnessing super-resolution techniques [4] including structured illumination microscopy (SIM) [5–7], stimulated emission depletion microscopy (STED) [8], photo-activation localization microscopy (PALM) [9, 10] or stochastic optical reconstruction microscopy (STORM) [11] to name a few. Improvements come when using quantum optics and single photon counting methods, which is the case for quantum image scanning microscopy [12] requiring *a priori* information of the number of photons emitted by a sample. In two photon absorption microscopy near simultaneous absorption of two photons allows for a better sample sectioning [13]. Its quantum counterpart, entangled two photon absorption [14, 15], replaces high energy light pulses with photon pairs, which widens the range of applicability due to significantly reduced intensity.

There has also been extensive discussion whether utilization of correlations between spatially separated light fields can lead to any resolution improvements [16–22]. This idea, known as ghost imaging (GI), was introduced in the late 80s by Klyshko *et. al.* [23] and experimentally demonstrated for

the first time in the mid 90s by Pittman *et. al.* [24]. The two correlated photons, traditionally called signal and idler, in the original scenario are generated in the process of spontaneous parametric down conversion (SPDC). The idler photon, used as a reference, when detected by a finite size detector heralds the presence of the signal photon, which is used to probe the sample. Similar scenarios exploiting thermal [25, 26] or pseudothermal light sources were proposed as well [27]. This concept was further developed in the context of fluorescence imaging by using spatially and temporally resolved detection [28], where the heralded signal photon is absorbed and then the fluorescence is emitted and detected. It is noted that the image of the sample is formed by coincidence detection of the reference and fluorescence photons. Although GI proved to be useful in the context of turbulence-free GI and GI in turbid media [29–32] or two-color imaging GI [18, 19, 33, 34], it was demonstrated that its resolution was fundamentally limited by the standard diffraction limit and does not enable sub-Rayleigh imaging [22]. Additionally, there are a few technical challenges to overcome in order to make this method practical. High brightness photon-pair sources are one of the elements, which are on the way [35]. Moreover, photon loss in the experimental setup is critical for these kind of experiments relying on the coincidence detection measurements, as the inefficiency scales quadratically with attenuation. However, achieving the diffraction limit requires the lateral spatial mode of the light entering the lens to be comparable with the size of its entrance aperture. This in turn introduces photon loss.

In this work we perform a systematic theoretical analysis of the signal photon's spatial mode profile in the framework introduced by Pittmann *et. al.* [24]. Using mathematical tools developed by Abouraddy *et. al.* [16], a general Gaussian form correlated biphoton wavefunction, describing a pair of photons produced in the SPDC process, is propagated through a finite size optical setup. The signal photon's spatial mode profile is studied in the heralding scheme and a comparison with the non-heralding scheme is provided. The impact of correlations on the lateral resolution is presented. Moreover,

\* Corresponding author. E-mail: kolenderski@umk.pl

it is shown that the diffraction limit can be approached even when the lateral mode of the probing photon entering the microscope objective is significantly smaller as compared to a typical situation involving laser light illumination. This is an important observation in the context of the photon loss discussion. Our conclusions are supported by numerical analysis and the derived analytical formulas. The calculations were made for realistic experimental parameters.

## II. FRAMEWORK

We assume that the probability density amplitude of generating a photon pair, where the idler and signal directions are given by  $\kappa_i, \kappa_s$ , reads:

$$\tilde{\psi}_{\text{in}}(\kappa_s, \kappa_i) \propto \exp \left( -\frac{1}{4} \left( \frac{\kappa_s^2}{\delta_s^2} + \frac{\kappa_i^2}{\delta_i^2} - \frac{2\kappa_i\kappa_s\rho}{\delta_i\delta_s} \right) \right), \quad (1)$$

where  $\delta_s, \delta_i$  stand for the mode profile radii of the signal and idler photons, and  $\rho$  is the Pearson coefficient, which is a measure of quantum correlation (entanglement) [36]. Here we assume that the aforementioned probability density amplitude is of a general Gaussian form. The relationship between Eq. 1 and the double-Gaussian approximation of the sinc-Gaussian biphoton wavefunction [21, 37], that is commonly used in this context, can be found by a direct calculation. The signal and idler photons generated in an SPDC source propagate through the optical setup depicted in Fig. 1. The idler photon, used as a reference, travels through a system of two lenses and is finally measured in the heralding plane by a single photon detector. The detection of the idler photon heralds the signal photon. The distances between the source, first lens, second lens and the heralding plane in the idler photon path are:  $d_{i1}$ ,  $d_{i2}$ , and  $d_{i3}$ , respectively. The distances between the source, first lens, microscope objective (MO) and the sample in the signal photon path are:  $d_{s1}, d_{s2}$  and  $d_{s3}$ , respectively. The focal lengths of the lenses in the idler arm are  $f_{i1}$  and  $f_{i2}$  and in the signal arm are  $f_s$  and  $f_{\text{MO}}$ . The free-space propagator that we apply here is of the form  $\exp(-i\pi(x' - x)^2/\lambda d)$ , where  $d$  is the propagation distance and  $\lambda$  is the wavelength. Similarly, the respective propagator for a lens of focal length  $f$  reads  $\exp(i\pi x^2/\lambda f)$ . All of the lenses are assumed to be thin and of finite aperture  $R_{i1}, R_{i2}$  for the idler and  $R_s, R_{\text{MO}}$  for the signal arm. All of the optical system parameters listed so far are combined into a parameter vector  $\vec{p}$  for convenience of notation. This allows us to symbolically represent the resulting wavefunction of the idler photon in the heralding detector plane and the signal photon at the sample plane in the following compact form,

$$\psi_{\text{out}}(x_s, x_i) = \int_{-\infty}^{\infty} dx'_s \int_{-\infty}^{\infty} dx'_i G_{\text{eff}}(x'_s, x'_i, x_s, x_i, \vec{p}) \psi_{\text{in}}(x'_s, x'_i). \quad (2)$$

Here,  $\psi_{\text{in}}(x'_s, x'_i)$  stands for the Fourier transform of the initial biphoton wavefunction given in Eq. (1) and

$G_{\text{eff}}(x'_s, x'_i, x_s, x_i, \vec{p})$  stands for the effective propagator including all free-space and lens propagations in both arms.

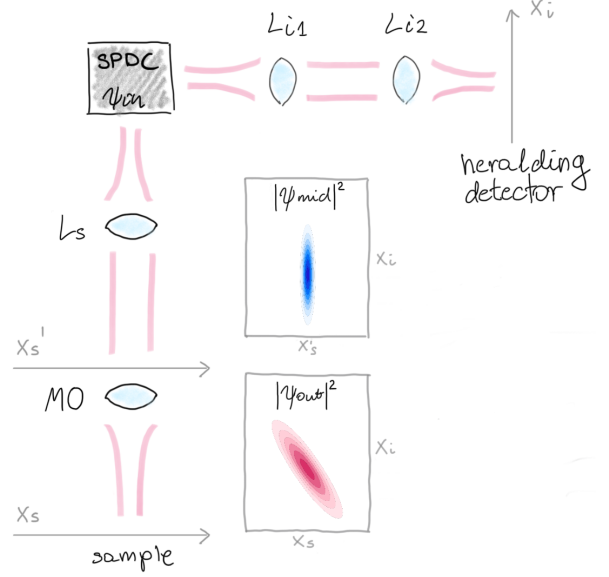


FIG. 1. **Experimental setup concept.** The input biphoton wavefunction,  $\psi_{\text{in}}$ , is generated in the SPDC source. The signal (idler) photon is propagated through free-space, signal (first idler) arm lens  $L_s$  ( $L_{i1}$ ), free-space, microscope objective MO (second idler arm lens  $L_{i2}$ ), again free-space and hits the sample (detector). The wavefunction propagated through free-space, first lens, and again free space on the signal arm and through the whole idler arm is denoted by  $\psi_{\text{mid}}(x'_s, x_i)$ , whereas the output wavefunction propagated through the whole signal and idler arms is denoted by  $\psi_{\text{out}}(x_s, x_i)$ . Typical joint probability distributions  $|\psi_{\text{mid}}(x'_s, x_i)|^2$  (blue) and  $|\psi_{\text{out}}(x_s, x_i)|^2$  (pink) computed for a correlation of  $\rho = 0.9$  are presented in the contour plots.

The biphoton wavefunction, as presented above, allows us to analyze the influence of the spatial entanglement on the performance of the single photon illumination. The probability density of a photon detection is a useful quantity, which can be computed based on the biphoton wavefunction and is directly proportional to the intensity of light. When the idler photon is measured in the heralding plane at position  $x_{iC}$  then the probability density of the signal photon detection at the sample plane at position  $x_s$  is given by

$$p_{\text{PLD}}(x_s; x_{iC}) = |\psi_{\text{out}}(x_s, x_{iC})|^2. \quad (3)$$

Here we consider a point like detector (PLD). Note that effects related to the use of a finite size detector (FSD) can be taken into account by integrating the probability density, given by the formula above, over the active area of the device. In turn, if the information about the idler photon's location is disregarded, the probability density,  $p_s(x_s)$ , of detecting the signal photon at position  $x_s$  can be found by formally tracing over the idler photon's position, which results in the following simple formula

$$p_s(x_s) = \int_{-\infty}^{\infty} dx_i |\psi_{\text{out}}(x_s, x_i)|^2. \quad (4)$$

The two formulas, Eqs. (3) and (4), constitute the framework for our analysis of the effects of entanglement and spatially resolved detection which can be used to control the illumination. In a similar way, we can compute the spatial mode intensity profile of the idler photon,

$$p_i(x_i) = \int_{-\infty}^{\infty} dx_s |\psi_{\text{out}}(x_s, x_i)|^2. \quad (5)$$

### III. SIMULATION RESULTS

To show the impact of spatial entanglement on the spatial mode profile of the signal photon, a simulation campaign was performed, where an experimentally achievable set of parameters was taken into account:  $f_s \in (30, 150)$  mm,  $f_{\text{MO}} = 2.5$  mm for the signal arm and  $f_{i1} = 30$  mm,  $f_{i2} = 1000$  mm for the idler arm. All of the lenses were placed at the respective focal distances, which corresponds to  $d_{s1} = f_s$ ,  $d_{s3} = f_{\text{MO}}$ ,  $d_{i1} = f_{i1}$  and  $d_{i3} = f_{i3}$ . The distances between the lenses were set to the same for both arms,  $d_{s2} = d_{i2} = 100$  mm. All of the lenses had finite apertures of the diameters:  $2 \cdot R_s = 2 \cdot R_{i1} = 25$  mm,  $2 \cdot R_{\text{MO}} = 8$  mm and  $2 \cdot R_{i2} = 50$  mm, which are typical values in an optical laboratory. The mode profiles of the photons generated by an exemplary SPDC source are also set to be equal,  $\delta_s = \delta_i = \frac{1}{4} \mu\text{m}^{-1}$ . We assume that the spectrum of the signal photon matches the absorption profile of a given sample and that the spectrum of the idler photon allows the use a free-space single photon detector. We consider energetically degenerate SPDC and the wavelengths of the idler and signal photons are set to  $\lambda_i = \lambda_s = \lambda = 532$  nm. Those parameters are kept fixed through the remaining part of the paper unless otherwise stated.

A typical simulation result illustrating the effect which is investigated here is given in Fig. 2. Panel (a) presents the joint spatial probability distribution,  $|\psi_{\text{out}}(x_s, x_i)|^2$ , computed for correlation coefficient  $\rho = 0.9$  and for  $f_s = 30$  mm. The gray gaussian curves in panels (b) and (c) are the probability distributions, as given in Eqs. (4) and (5), of the idler and signal photon detection respectively, when information about the other photon from the pair is disregarded. When the idler photon is detected by a PLD at the point in the center,  $x_{iC} = 0 \mu\text{m}$ , or at a side  $x_{iC} = -96 \mu\text{m}$  (marked on panel (b) by dark and light blue lines, respectively), then the spatial profile of the signal photon is given by a function, drawn in the same color on panel (c).

Entanglement assisted wavepacket narrowing can be seen when comparing the non-heralded signal photon spatial mode profile (gray curve) with the respective heralded signal photon's profile (blue curves). The center location of the heralded signal photon,  $x_{sC}$ , shown in panel (c), follows the central position of the heralding detector,  $x_{iC}$ , which obeys the relation

$$x_{sC} = -\frac{f_{i1} f_{\text{MO}}}{f_s f_{i2}} \frac{\delta_i}{\delta_s} \rho \cdot x_{iC}. \quad (6)$$

Note that the formula presented above was obtained for a PLD, however, an experimentally available FSD with an active area diameter on the order of 30  $\mu\text{m}$  was tested as well.

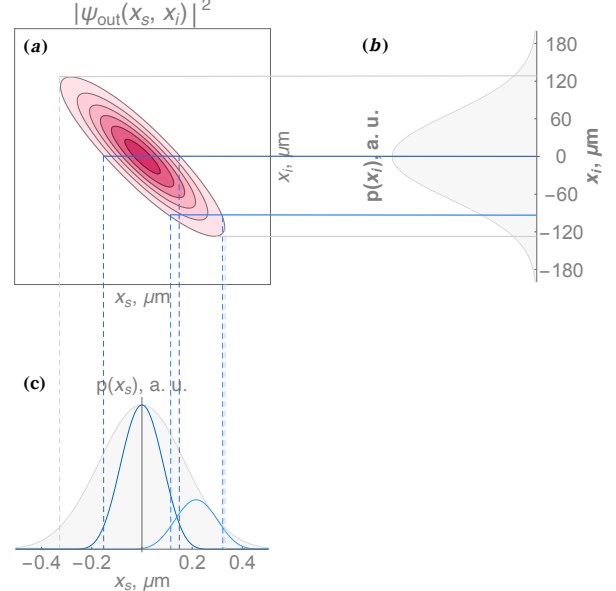


FIG. 2. **Entanglement assisted wavepacket narrowing** (a) Example joint probability distribution,  $|\psi_{\text{out}}(x_s, x_i)|^2$ . The contours are equally spaced every 10%. (b) Marginal probability of detecting the idler photon when neglecting information about the signal photon,  $p_i(x_i)$ . (c) Marginal probability of detecting the signal photon when neglecting information regarding idler photon,  $p(x_s)$  (gray). Heralded (PLD) signal photon spatial mode profiles (blue). The plots were generated for  $\rho = 0.9$  and  $f_s = 30$  mm. The horizontal, solid lines at  $x_i = 0 \mu\text{m}$  and  $x_i = -96 \mu\text{m}$  represent the detector's location.

We did not find an analytical formula when assuming the use of an FSD, but numerical analysis gave a very similar slope as for the PLD.

### IV. LATERAL RESOLUTION ANALYSIS

This method can serve as an alternative way of scanning in a fluorescence microscopy setting. Instead of moving the sample while keeping the MO fixed, both the sample and the MO can be fixed and the position of the heralding detector can change [28]. Such a scheme requires a large area, single-pixel detector along with an appropriate spectral filter on the heralded arm to collect the fluorescence from the sample illuminated with heralded single photons. Note that these kind of detectors are named "bucket detectors" in the literature on GI. Interestingly, the image in this case would be created at the heralding detector when a coincidence detection on both the detectors, fluorescence and heralding, was registered.

There are some conditions, which must be met to approach the diffraction limit. This can be understood from simulation results for a complete set of parameters given in Fig. 3. The X-axis of each plot represents the width of the spatial mode profile before the MO,  $\sigma_{\text{mid}}$ . Here, the  $\sigma_{\text{mid}}$  width is defined as the radius of an iris able to transmit 99% intensity of the photon profile described by the wavefunction  $\psi_{\text{mid}}$ . The left Y-axis represents the FWHM of the Gaussian fit to the out-

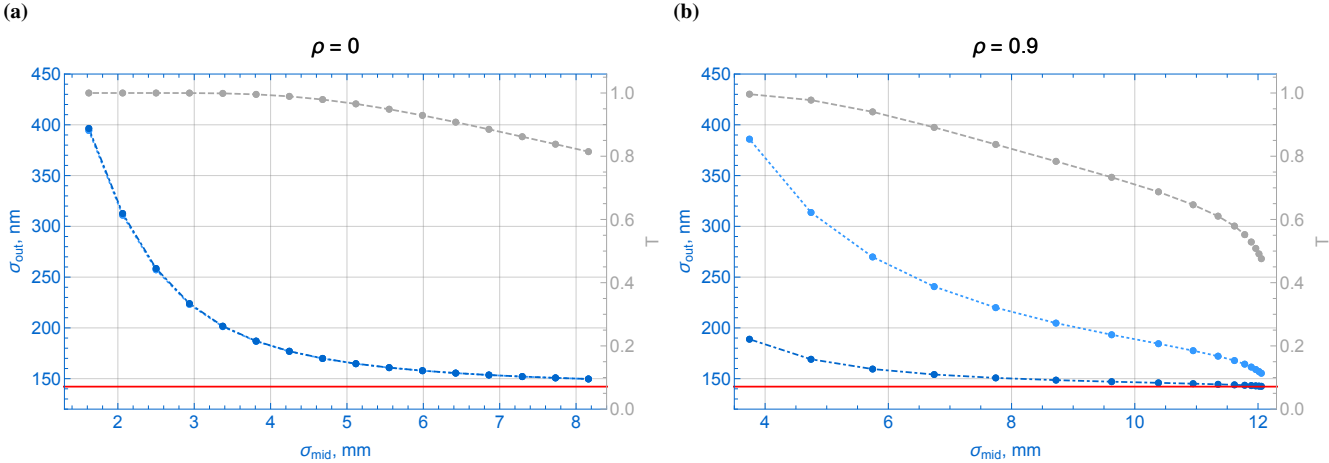


FIG. 3. **Approaching the diffraction limit.** Width (transmission) of the signal photon wavepacket after propagation through the whole optical setup as a function of the width of the signal photon wavepacket before the MO,  $\sigma_{\text{out}}(\sigma_{\text{mid}})$  ( $T(\sigma_{\text{mid}})$ ).  $\sigma_{\text{out}}$  width stands for the FWHM of the Gaussian fit to the output wavepacket whereas  $\sigma_{\text{mid}}$  width is defined as the radius of an iris able to transmit 99% intensity of the photon profile described by the wavepacket  $\psi_{\text{mid}}$ . Light blue, dotted:  $\sigma_{\text{out}}(\sigma_{\text{mid}})$  in the non-heralded scenario. Dark blue, dotted-dashed:  $\sigma_{\text{out}}(\sigma_{\text{mid}})$  in the heralded scenario. Gray, dashed:  $T(\sigma_{\text{mid}})$ . The diffraction limit is marked as a red solid line which was obtained by propagating a delta function,  $\delta(x)$ , through the optical setup and from a Gaussian fit the width of  $\sigma_{\text{out},\delta(x)} = \sqrt{2\ln 2} \cdot \sigma_{\delta(x)} = 142.163$  nm was obtained, where  $\sigma_{\delta(x)}$  is the Gaussian function parameter. The simulation was run for  $f_s \in (30, 150)$  mm and  $\rho = 0, 0.9$ .

put spatial mode profile,  $\sigma_{\text{out}}$ , whereas the right Y-axis stands for the wavepacket transmission through the MO. Three figures of merit are presented on each plot as a function of the spatial mode profile's width before the MO: 1) output spatial mode profile width,  $\sigma_{\text{out}}^{\text{nh}}$ , in the non-heralding scenario (light blue, dotted), 2) output spatial mode profile width,  $\sigma_{\text{out}}^{\text{h}}$ , in the heralding, PLD scenario (dark blue, dotted-dashed), and 3) transmission of the wavepacket through the MO (gray, dashed). In the case where the photon pair features no entanglement,  $\rho = 0$ , one can observe that the data sets for both, heralding and non-heralding scenarios, overlap. Moreover, what is obviously expected, a bigger spatial mode entering the MO corresponds to a smaller resulting spatial profile in the focal point. Entanglement makes the difference as can be seen in Fig. 3(b). The monotonicity of the  $\sigma_{\text{out}}(\sigma_{\text{mid}})$  relation is preserved, but the sets of points for the heralding and non-heralding scenarios do not overlap any more. It is seen that for a given width of the spatial mode before the MO,  $\sigma_{\text{mid}}$ , one cannot achieve in the non-zero correlations case and non-heralding scenario as small of spot size as in the zero-correlations one. To approach the diffraction limit, heralding is necessary. For instance,  $\rho = 0.9$  for  $f_s = 30$  mm leads to the resolution of 385.88 nm in the non-heralding scenario, whereas 188.84 nm resolution is obtained when heralding. Nevertheless, this result itself is interesting from the fundamental point of view. It shows that it is not sufficient to have the beam's spatial mode of a comparable size with the focusing lens aperture. In the case of a correlated biphoton wavefunction, a heralding scenario has to be additionally applied to approach the diffraction limit.

In Fig. 4, the joint probability density,  $|\psi_{\text{mid}}(x'_s, x_i)|^2$ , and the phase,  $\text{Arg}(\psi_{\text{mid}}(x'_s, x_i))$ , of the wavefunction before the MO are given for  $f_s = 150$  mm and 30 mm. Firstly, the

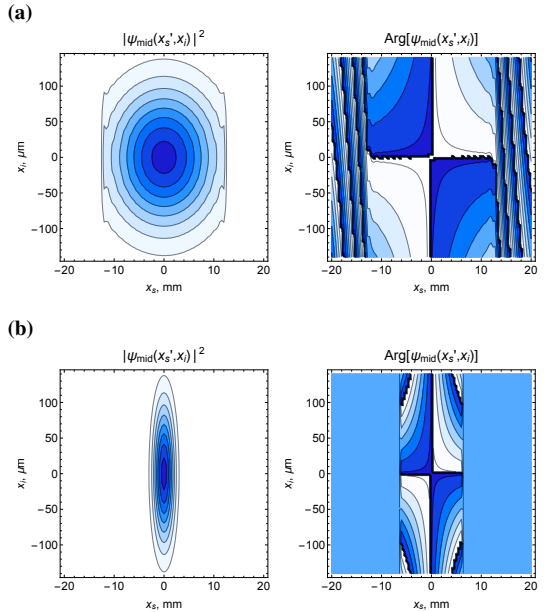


FIG. 4. **Spatial mode and phase profiles of the biphoton wavefunction before the MO.**  $|\psi_{\text{mid}}(x'_s, x_i)|^2$  and  $\text{Arg}(\psi_{\text{mid}}(x'_s, x_i))$ , for  $\rho = 0.9$  and: (a)  $f_s = 150$  mm and (b)  $f_s = 30$  mm.

impact of the finite aperture of the first signal arm lens can be noticed ( $R_s = 12.5$  mm) in the non-gaussian shape of  $|\psi_{\text{mid}}(x'_s, x_i)|^2$  and in the cutting of all the plots at 12.5 mm. Secondly, contrary to the joint probability for the output wavefunction,  $|\psi_{\text{out}}(x_s, x_i)|^2$ , no correlations are observed in the joint probability of the wavefunction before the MO,  $|\psi_{\text{mid}}(x'_s, x_i)|^2$ . They become apparent, however, in its phase,

$\text{Arg}(\psi_{\text{mid}}(x'_s, x_i))$ . We conclude that not only the width of the spatial mode profile entering a lens has an impact on the beam waist in the focal point but also the phase correlations of the entering wavepacket matter as well. In this sense, a heralding scheme has a similar effect as the wavefront correction made by adaptive optics [7].

One more feature of the results presented in Fig. 3 should be stressed. What can be observed in Fig. 3 (b) is that in the case of non-zero correlations and a non-heralding scenario (light blue, dotted), the diffraction limit can be approached with the transmission below 0.5. When the signal is heralded (dark blue, dotted-dashed), the diffraction limit with a much greater transmission, above 0.9 is approached. This is an important observation in the context of applications making use of correlated photon pairs, where even small losses are detrimental. In practical implementation a single photon avalanche diode (SPAD) array could be used [38]. Then, the efficiency would be limited by factors including the detection efficiency and the fill factor of the detector array.

## V. CONCLUSIONS

Summarizing, the limits of entangled assisted wavepacket narrowing were numerically analyzed. It was shown that the spatial mode profile of the signal photon can be narrowed when its spatially separated twin photon is detected by a point-like detector. The results were obtained for an experimentally

accessible set of parameters. Also, it was tested that the application of a finite-size detector lead to similar results. At the same time, however, one has to be aware of the accompanying limitations such as the impact of the phase correlations of the wavefunction entering a lens at the diffraction limit that can be achieved. Additionally, it was observed that in the case of correlated photon pairs this method enables approaching the diffraction limit with a much better transmission. This is a relevant aspect when discussing applications of correlated photon pairs, where high transmission is a critical performance parameter.

## ACKNOWLEDGEMENTS

PK acknowledges financial support from the Foundation for Polish Science (FNP) (project First Team co-financed by the European Union under the European Regional Development Fund), MG acknowledges financial support from the National Science Centre, Poland (NCN) (Preludium 18 grant no. 2019/35/N/ST2/03443) and CJP acknowledges financial support from the Brandon University Research Committee. All the authors acknowledge support by the National Laboratory of Atomic, Molecular and Optical Physics, Torun, Poland. MG and PK are grateful for insightful discussions with Sylwia M. Kolenderska.

---

[1] E. Hecht, *Optics* (Addison Wesley Publishing Company, 2002) p. 698.

[2] B. E. A. Saleh and M. C. Teich, *Fundamentals of Photonics* (John Wiley & Sons, INC, 2019).

[3] D. S. Simon, G. Jaeger, and A. V. Sergienko, *Quantum Metrology, Imaging, and Communication* (Springer, Cham, 2016).

[4] J. Vangindertael, R. Camacho, W. Sempels, H. Mizuno, P. Dedecker, and K. P. F. Janssen, *Methods and Applications in Fluorescence* **6**, 022003 (2018).

[5] M. G. Gustafsson, *J Microsc* **198**, 82 (2000).

[6] N. Ji, D. E. Milkie, and E. Betzig, *Nat. Methods* **7**, 141 (2009).

[7] K. Philipp, F. Lemke, S. Scholz, U. Wallrabe, M. C. Wapler, N. Koukourakis, and J. W. Czarske, *Sci. Rep.* **9** (2019), 10.1038/s41598-019-45993-4.

[8] S. W. Hell and J. Wichmann, *Opt. Lett.* **19**, 780 (1994).

[9] E. Betzig, G. H. Patterson, R. Sougrat, O. W. Lindwasser, S. Olenych, J. S. Bonifacino, M. W. Davidson, J. Lippincott-Schwartz, and H. F. Hess, *Science* **313**, 1642 (2006).

[10] S. T. Hess, T. P. Girirajan, and M. D. Mason, *Biophys. J.* **91**, 4258 (2006).

[11] M. J. Rust, M. Bates, and X. Zhuang, *Nat. Methods* **3**, 793 (2006).

[12] R. Tenne, U. Rossman, B. Rephael, Y. Israel, A. Krupinski-Ptaszek, R. Lapkiewicz, Y. Silberberg, and D. Oron, *Nature Photonics* **13**, 116 (2019).

[13] B. Mollow, *Phys. Rev.* **175**, 1555 (1968).

[14] H.-B. Fei, B. M. Jost, S. Popescu, B. E. A. Saleh, and M. C. Teich, *Physical Review Letters* **78**, 1679 (1997).

[15] B. Dayan, *Phys. Rev. A* **76**, 043813 (2007).

[16] A. F. Abouraddy, B. E. Saleh, A. V. Sergienko, and M. C. Teich, *JOSA B* **19**, 1174 (2002).

[17] I. F. Santos, M. A. Sagioro, C. H. Monken, and S. Padua, *Conf. Quantum Electron. Laser Sci. - Tech. Dig. Ser.* **89**, QMH5/1 (2003).

[18] M. H. Rubin and Y. Shih, *Phys. Rev. A - At. Mol. Opt. Phys.* **78** (2008).

[19] K. W. C. Chan, M. N. O'Sullivan, and R. W. Boyd, *Phys. Rev. A - At. Mol. Opt. Phys.* **79**, 1 (2009).

[20] B. I. Erkmen and J. H. Shapiro, *Phys. Rev. A - At. Mol. Opt. Phys.* **78**, 1 (2008).

[21] M. L. Zhong, P. Xu, L. L. Lu, and S. N. Zhu, *Sci. China Physics, Mech. Astron.* **59** (2016).

[22] P.-A. Moreau, E. Toninelli, P. A. Morris, R. S. Aspden, T. Gregory, G. Spalding, R. W. Boyd, and M. J. Padgett, *Opt. Express* **26**, 7528 (2018).

[23] D. N. Klyshko, *Photons Nonlinear Optics* (Gordon & Breach, 1988).

[24] T. B. Pittman, Y. H. Shih, D. V. Strekalov, and A. V. Sergienko, *Phys. Rev. A* **52**, R3429 (1995).

[25] R. S. Bennink, S. J. Bentley, and R. W. Boyd, *Phys. Rev. Lett.* **89**, 113601 (2002).

[26] A. Gatti, E. Brambilla, M. Bache, and L. A. Lugiato, *Phys. Rev. Lett.* **93**, 1 (2004).

[27] F. Ferri, D. Magatti, A. Gatti, M. Bache, E. Brambilla, and L. A. Lugiato, *Phys. Rev. Lett.* **94**, 2 (2005).

[28] G. Scarcelli and S. H. Yun, *Optics Express* **16**, 16189 (2008).

[29] W. Gong and S. Han, *Opt. Lett.* **36**, 394 (2011).

- [30] R. E. Meyers, K. S. Deacon, A. D. Tunick, and Y. Shih, *Appl. Phys. Lett.* **100** (2012).
- [31] P. B. Dixon, G. A. Howland, K. W. C. Chan, C. O'Sullivan-Hale, B. Rodenburg, N. D. Hardy, J. H. Shapiro, D. S. Simon, A. V. Sergienko, R. W. Boyd, and J. C. Howell, *Phys. Rev. A - At. Mol. Opt. Phys.* **83**, 5 (2011).
- [32] M. Bina, D. Magatti, M. Molteni, A. Gatti, L. A. Lugiato, and F. Ferri, *Phys. Rev. Lett.* **110**, 1 (2013).
- [33] R. S. Aspden, N. R. Germell, P. A. Morris, D. S. Tasca, L. Mertens, M. G. Tanner, R. A. Kirkwood, A. Ruggeri, A. Tosi, R. W. Boyd, G. S. Buller, R. H. Hadfield, and M. J. Padgett, *Optica* **2**, 1049 (2015).
- [34] Z. Li, N. Medvedev, H. N. Chapman, and Y. Shih, *J. Phys. B At. Mol. Opt. Phys.* **51** (2018).
- [35] E. Meyer-Scott, N. Prasannan, C. Eigner, V. Quiring, J. M. Donohue, S. Barkhofen, and C. Silberhorn, *Opt. Express* **26**, 32475 (2018).
- [36] C. J. Pugh, P. Kolenderski, C. Scarcella, A. Tosi, and T. Jennewein, *Opt Express* **24**, 20947 (2016), 1606.04110.
- [37] J. Schneeloch and J. C. Howell, *J. Opt. (United Kingdom)* **18** (2016).
- [38] F. Guerrieri, S. Tisa, A. Tosi, and F. Zappa, *IEEE Phot. Journal* **2**, 759 (2010).